World Journal of Advanced Engineering Technology and Sciences
eISSN: 2582-8266
Cross Ref DOI: 10.30574/wjaets
Journal homepage: https://wjaets.com/

(RESEARCH ARTICLE)

Check for updates

Preparation and characterization of molybdenum trioxide/poly(3,4-ethylenedioxythiophene): Polystyrene sulphonate nanocomposites for electrochromic application.

Sagir Ziya'ulhaq [1,*] and TH Darma [2]

[1] *Department of Physics, Isa Kaita College of Education Dutsin-ma, Katsina State, Nigeria.*
[2] *Department of Physics, Bayero University Kano, Kano State, Nigeria.*

World Journal of Advanced Engineering Technology and Sciences, 2023, 10(01), 108–121

Publication history: Received on 14 August 2023; revised on 23 September 2023; accepted on 25 September 2023

Article DOI: https://doi.org/10.30574/wjaets.2023.10.1.0258

Abstract

Electrochromic processes are mostly characterized by colour change arising from the energy of a chemical reaction involving electron transfer. Transition metal oxides of tungsten, molybdenum, iridium, and nickel show the most intense Electrochromic colour changes and photochemical stability of about 100 cycles compared to organic electrochromes which are susceptible to photochemical degradation. The prospect of conjugated polymers (comprising of metal oxides and polymers) has opened a new dimension on improving the Electrochromic performance of the transition metal oxides. In this work, solution growth methods were employed in preparing a MoO_3/PEDOT: PSS composite layer by adding PEDOT: PSS into MoO_3 aqueous dispersion resulting in an electrostatic interaction between MoO_3 and PEDOT: PSS for electrochromic application. This composite has shown a long-term stability up to more than 550 cycles which shows higher potential specific capacitance than WO_3/PEDOT: PSS. This approach has significantly improved the stability issue of MoO_3 and enhances the potential of MoO_3-based materials for electrochromic applications. The semi crystalline nature of MoO_3-300 °C was further proved by FE-SEM observation of the MoO_3 nanoparticles. The particle size shown in the images corresponds with FE-SEM result and polycrystalline structure was observed under high magnification. The polycrystalline nature of the MoO_3 particles favors their electrochemical stability, while their small size facilitates their effective interactions with PEDOT: PSS. The electrochemical properties of MoO_3, PEDOT: PSS and composite were further studied by cyclic voltammetry (CV) from -1 V to +1 V. MoO_3 has a broad oxidation peak at -0.43 V and no obvious reduction peak in this range. PEDOT: PSS has an oxidation peak at -0.02 V and a reduction peak at -0.55 V. In the composite, the peak at -0.43 V becomes a shoulder and a new pair of redox peaks appear at -0.18 V/-0.09 V.

Keywords: Electrochromism; ECD; Transition Metals; MoO_3; PEDOT: PSS; Conjugated polymers; WO_3

1. Introduction

Electrochromism is the phenomenon of the reversible color change of thin films under an applied voltage. Electrochromism was first reported on inorganic metal oxides. After decades of research, some inorganic electrochromic materials have been developed and commercialized on a large scale. However, inorganic electrochromic materials have many disadvantages, such as slow response time, high cost and difficulty in processing. Currently, the use of conducting polymers in electrochromism has attracted much attention due to their high optical contrast ratio, fast response speed, low applied potential, and diverse color possibilities [34]. The ability to change colors in thin films is important for applications such as smart windows, rearview mirrors, and gas sensors. During the color change, intercalation and deintercalation of ions (H^+, Li^+, Na^+) takes place, controlled by the applied voltage between two transparent conducting oxide (TCO) layers [4]. The reversible color change results from the generation of different

* Corresponding author: Sagir Ziya'ulhaq; ORCID: 0000-0002-7035-8521

electronic absorption bands in the visible range when switching between redox states [28]. The electrochromism of conjugated polymers is the result of redox reactions, which are a p-doping/de-doping process [26]. The electrochromic materials are either oxidized/reduced with the introduction of ions and charges, so that the optical properties of the materials change, resulting in a color change [31]. A material colored in the reduced state is a cathodically colored material, and a material colored in the oxidized state is an anodically colored material. In the oxidized state, the conjugated polymer is doped with counter anions (p-doping) and has a delocalized electron band. Upon reduction, the escape of counter anions or the incorporation of cations (un-doping) restores the band structure of the conjugated polymer. Therefore, the redox reactions of conjugated polymers create and remove the new optical absorption band, causing color changes. Electrochromic conjugated polymers have advantages like high contrast, fast switching speed, flexibility, and good process ability [2]. For practical applications, fast response time and low operational voltage are necessary performance indexes for electrochromic displays [22]. A typical electrochromic device is made up of three components: electrode, electrochromic material, and electrolyte. Electrochromic materials are coated on the electrodes and separated by electrolyte in the electrochromic device. Optical contrast, which is the variation in transmittance between colored and bleached states, is the most important parameter of an electrochromic device. Other parameters like switching time and long-term stability are also concerned in electrochromic materials [16].

Electrochromic materials are new types of functional materials that can be used for energy-saving and electrochromic devices (ECDs), which have attracted great attention from researchers. Electrochromic material changes color through an electrochemical reaction in a persistent but reversible manner. Electrochromic materials are applied to the electrodes and separated by electrolyte in the electrochromic device. Transitioning between different valence states of transition metals makes them a promising option for electrochromics as they have high optical contrast and good long-term stability due to their crystallinity and environmental stability, but longer switching time due to their poor conductivity [33]. In the last decade, electrochromic devices using electrochemically active conjugated polymers have been extensively studied [28]. Two types of commonly used electrochromic materials are transition metal oxides and conjugated polymers. Transition metal oxides such as WO_3 and MoO_3 are well studied for electrochromism [1]. Conjugated polymers such as polyaniline (PANI) and poly(3,4-ethylenedioxythiophene): polystyrene sulfonate (PEDOT: PSS) are also electrochromic as they have different oxidation states that show different colors. Compared to transition metal oxides, electrochromic conjugated polymers have advantages such as faster switching speed, flexibility, multicolor, and low cost [8]. However, they usually suffer from stability issues due to over-oxidation [19].

PEDOT: PSS is electrochromic as it exhibits reversible electrochemical oxidation and reduction. The color of PEDOT: PSS can change reversibly from transparent light blue to dark blue. Kawahara et al. reported an electrochromic device with about 42% contrast constructed by controlling the thickness of PEDOT: PSS [35]. Teherani et al. fabricated PEDOT: PSS-based electrochromic paper display utilizing the flexibility of PEDOT: PSS [18]. Gomes et al. increased the conductivity of PEDOT: PSS used in electrochromic applications by adding conductive particles to improve performance [16]. In general, the optical contrast could be improved by increasing the thickness, but the switching time is affected since the ion transport is hampered by the cumbersome morphology. Since each type of material has its own strengths and weaknesses, a composite material is a good option with the potential to show the benefits of both components. Composites based on conjugated polymers have been extensively studied for electrochromic applications. The main reason is to take advantage of the conductivity and flexibility of conjugated polymers. For example, the charge transfer of WO_3/poly(4-(2,3-dihydrothieno[3,4-b]- [1,4] dioxin-2-yl-methoxy)-1-butanesulfonic acid) (PEDTS) composite was due to being improved to the good conductivity of PEDTS [36]. A flexible electrode, Ag grid/PEDOT: PSS, was fabricated and used in bendable electrochromic applications [9].

Researchers have made great efforts to improve the performance of electrochromic devices, including their staining efficiency, response time, and cycling stability [27]. The performance of the improved devices could be due to improved charge injection and better compatibility with the hydrophobic nature of the organic layer. The electrochromic devices offer a variety of advantages, including no-load memory, low power consumption, wide vision, safety, and adjustable color depth [34]. Electrochromic devices can exhibit reversible color changes induced by electrical energy and the resulting redox electrochemical reactions of materials. Due to unique features such as reversible change of optical properties including color, reflection, and transmittance under the behavior of voltage pulses, the electrochromic devices have received enormous interest regarding their use in various applications, such as automobile sunroofs and mirrors, electronic displays, intelligent windows, flexible displays, electrochromic skins, and sensors [29]. Typical ECDs include the sandwich structure consisting of five functional layers: the electrolyte layer, two transparent conductive layers, and the cathodic electrochromic (EC) layer and the anodic electrochromic layer [5]. The changes in the optical states are consequences of a change in the electronic state because of electron transfer between the electrochromic material and the electrode. ECDs offer many advantages over traditional displays, including low operating voltage, memory effects, color variation, and visibility in sunlight. In electrochromic devices, the transparent materials are colored when an electric potential difference is applied to them [27]. Therefore, ECDs are expected to achieve

applications in information displays or in light-modulating devices such as smart windows, switchable mirrors, electronic papers, and chemical sensors. Traditional ECDs consist of non-metallic EC material (e.g. poly (ethylene oxide), polyvinylidene difluoride, WO_3, $Ir(OH)_3$, NiO) [12]. A WO_3 nanoparticle-coated Ag/PEDOT: PSS is reported to exhibit electrochromism and a specific capacity of 221 F g^{-1} at 1 A g^{-1} [8]. Due to the lower molar mass, MoO_3 has a higher specific capacity than WO_3.

MoO_3 is an electrochromic material that has higher apparent contrast and better open circuit memory than the most used WO_3. However, MoO_3 is not commonly used as the main component of an electrochromic material due to its low conductivity in the fully oxidized state and poor long-term stability. So far, electrochromic materials based on MoO_3 only show a stability of about 100 cycles. It is reported that good conductivity and stability of up to 150 cycles was achieved by a stacked MoO_3/Ag/MoO_3 film constructed to form a dielectric-metal-dielectric structure by reducing the thickness of each layer has been adjusted [15]. However, such layered structures have been fabricated by electron beam evaporation, which requires expensive equipment. At present, a simple method to fabricate a MoO_3-based electrochromic material with good performance and long-term stability remains a challenge. In this work, an electrochromic MoO_3/PEDOT: PSS composite was prepared by adding PEDOT: PSS into an aqueous MoO_3 dispersion, resulting in an electrostatic interaction between MoO_3 and PEDOT. The composite produced has demonstrated long-term stability up to more than 550 cycles, demonstrating a higher potential specific capacity than WO_3/PEDOT: PSS. This approach has significantly improved the MoO_3 stability problem and increases the potential of MoO_3-based materials for electrochromic applications. It is also proven that both electron and ion transport play important roles in capacitive performance.

1.1. Theoretical background

The schematic of an electrochromic glass is shown in Figure 1. It consists of two transparent glasses with a five-layer electrochemical cell in between. A solid or polymer electrolyte is used in commercially available electrochromic glasses. The thickness of the five-layer structure is about 1 (m) in the first version and about 0.75 mm in the second version [34]. The central part of the electrochemical cell, i.e., an ion conductor (electrolyte), can be made of an organic material (a sticky polymer) or an inorganic compound (usually an oxide film) Ions, protons + or Li^+, are small enough to remain mobile the other surface of the ion conductor is in contact with a layer that plays the role of an ion source.

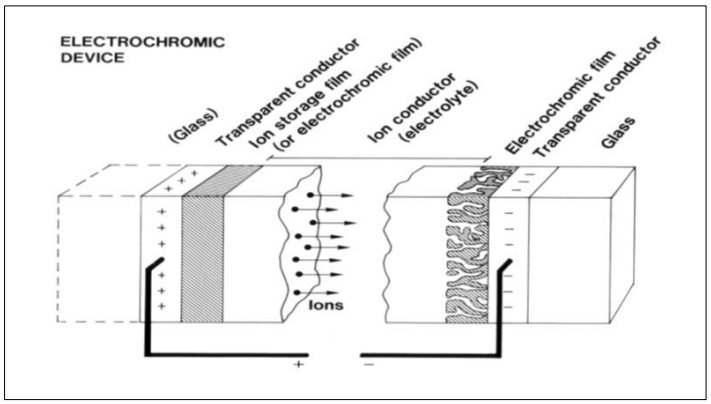

Figure 1 Generic EC device configuration showing a multilayer structure on a single substrate (monolithic design) and, alternatively, such a structure interposed between two substrates (polymer laminate design) [30]

When a constant voltage of about 1 V is applied between electrically conductive coatings, ions from an ion source are injected into the electrochromic layer. Electrons are injected from the electrically conductive coating into the cathode electrochromic layer. Electrons induce a change in optical absorption and layer color. An additional effect, namely a color change of the anode layer during the extraction of ions, is achieved in an ideal situation where this layer plays not only the role of an ion source, but also the role of an electrochromic layer [10].

The optical contrast of an electrochromic material measures the degree of optical change between its redox states. For electrochromic purposes, a high optical contrast is favored as it signifies a highly discernible color or transmissivity change. Optical contrast is typically defined as the absolute percent transmittance difference (Δ%T) between the fully oxidized and fully reduced states as given in the equation below:

$$\Delta\%T = T_{ox} - T_{red} \quad \text{.....(1)}$$

The switching time measures how fast the electrochromic material switches between the redox states in response to an applied potential. For colored-to-bleached types of electrochromic materials, there are two distinct processes occurring in the color change (transition from colored to bleached states and vice versa). The coloration time, corresponds to the speed of the coloration process whereby the electrochromic material changes from a state with a higher percent transmittance to a state with a lower percent transmittance [25]. On the other hand, the bleaching time, t_b corresponds to the speed of the bleaching process whereby the electrochromic material changes from a state with a lower percent transmittance to a state with a higher percent transmittance. Predominantly, the switching time is defined as the time taken for the electrochrome to switch to 95% of its full switch. Even though a value of 95% is typically chosen as the human eye cannot detect the remaining 5% of colour change, calculations based on 75 or 90% of the total transmittance changes are not uncommon [2]. Other approaches to quantify the switching times include measurements of the duration needed for part or all the necessary charges to be injected.

The optical memory (or idle memory) of an electrochrome measures the length of time that the electrochrome can retain its last redox state after removal of the applied electrical bias. For any electrochrome, the extent of its optical memory depends on the length of time the electron can be trapped in the specific redox state. The stability of an electrochromic or electrochromic device evaluates its ability to maintain electrochromic performance under repeated redox cycles and doping/un-doping processes. The measurement and evaluation of electrochemical stability and device durability differ among different research groups, which makes it difficult and difficult to directly evaluate and compare the performance of electrochromes [32]. A common approach to measuring stability is to record the number of redox cycles that the electrochrome or device can endure before significant degradation or a specified percentage drop in optical contrast occurs.

The amount of electrochromic colour formed by the charge consumed is characteristic of the electrochrome. Its value depends on the wavelength chosen for study. The optimum value is the absorbance formed per unit charge density measured at λ_{max} of the optical absorption band. The coloration efficiency η is defined as:

$$Abs = Log (I_o/I) = \eta Q \ldots\ldots\ldots\ldots\ldots\ldots (2)$$

where Abs is the absorbance formed by passing a charge density of Q. A graph of Abs against Q accurately gives η as the gradient [20].

The proportionality factor, the coloring efficiency, is a quantitative measure of the electrochemically formed color. For an ECD in transmisSsion mode, it is measured as the change in optical absorbance (Abs).

$$\eta = \Delta(Abs) / Q \quad \ldots\ldots\ldots\ldots\ldots\ldots (3)$$

The proportionality factor is obviously independent of the optical path length l within the sample. EC measurements are commonly used to obtain the three performance characteristics of electrochromic materials/devices (ECD). These are staining efficiency (CE), optical density change (OD), and optical modulation (T). The CE is a parameter used to assess the power consumption of the electrochromic material. It is defined as the change in optical density per unit injected/ejected charge and is given by Equation (4) in units of cm^2c^{-1}. Organic materials generally have higher staining efficiency than inorganic ones due to higher molar absorbance [26].

$$CE;\ \eta = \frac{\log Tox - Tred}{q/A} \quad \ldots\ldots\ldots\ldots\ldots\ldots\ldots (4)$$

OR

$$CE = \Delta OD/\Delta Q \quad \ldots\ldots\ldots\ldots\ldots\ldots (5)$$

where T_{ox} and T_{red} refer to the percent transmittance (%T) of the bleached and colored states respectively, q the charge consumed during the process in Coulombs (C), and the active area (A) of the electrochrome in cm^2.

CE values can be calculated at various levels of percent transmission change such as 90%, 95%, or 98%. For electrochromic applications, a higher CE value is advantageous as it means that a high optical change can be achieved with a small amount of charge and hence lower power consumption and higher energy efficiency [3]. While CE is an intrinsic property of electrochromism, it is wavelength dependent. The change in optical density is defined by the equation:

$$\Delta OD = \log (T_b/T_c) \text{.....(6)}$$

where Tb and Tc are the transmittance values of the film in bleached and colored states, respectively.

The optical modulation is the difference between the transmittance values of the device for the specific wavelength both in bleached and colored states.

$$(\Delta T = T_b - T_c) \quad \text{.....(7)}$$

The higher CE indicates that ECDs provide large optical modulation with a small amount of inserted or extracted ions/charges. Because a small amount of charge insertion or extraction rate improves the cyclic stability of the EC film, which is a crucial parameter to construct a durable, long-life EC device. There are also other parameters related to electrochromic devices such as: B. Write-erase efficiency, defined as the percentage of color originally formed that can subsequently be bleached; Open-circuit memory, which can be described as the time it takes to retain color after the external potential has been removed in the colored state.

2. Material and methods

This section lists all materials used and describes the method used to prepare crystalline MoO_3 nanoparticles and the method used in the electrical and physical analysis of the MoO_3/PEDOT: PSS composite material. It also describes the process used to fabricate the MoO_3/PEDOT: PSS composite.

ITO-coated glass (< Ω/sq[1], Sigma Aldrich), PEDOT: PSS (1.3 wt% dispersion in water, conductive grade), lithium perchlorate ($LiClO_4$, ACS reagent, ≥95.0%), propylene carbonate (PC, anhydrous, 99.7%), and Molybdenum powder (99%), were purchased from Sigma-Aldrich. Ethanol (99.9%) were purchased from Merck Germany. 30% H_2O_2 were purchased from Sigma-Aldrich. Acetone (technical grade) and isopropyl alcohol (IPA, technical grade) were purchased from Zhuhai Kaivo Optoelectronic Technology Co. Ltd. China. All chemicals were used as received.

The experiment of this research was based on the depositing transporting layer MoO_3 and PEDOT: PSS in formation of MoO_3/PEDOT: PSS solid electrochromic layer via electrostatic interaction.

2.1. Preparation of Crystalline MoO_3 Nanoparticles

2g of molybdenum powder was slowly added to 50 mL 30% H_2O_2 solution with continuous stirring. 50 mL of ethanol was added after stirring for 3 h. The solution was stirred for 10 h and then a Pt sheet was placed in the solution for 48h to remove excess H_2O_2 and obtain the clear precursor. The precursor was then dried at 70 °C for 3 h, and then annealed to 300 °C for 2 h in a tube furnace with ramp of 5 °C/min. The precursor without annealing was dried at 60 °C as a reference sample for characterization tests.

2.2. Cleaning of ITO Substrate

Indium-doped tin oxide (ITO)-coated glass sheets (< Ω/sq[1], Sigma Aldrich) were cut 20 × 30 mm and patterned by Cleaning the surface. Firstly, the active area of ITO sheets was tested. The ITO were cleaned with soap water, and then ultrasonic bath with de-ionized (DI) water, acetone, ethanol, and IPA consequently, and finally with DI water again for 10 minutes each and then dried with nitrogen gas. Finally, the ITO glass was subjected to oxygen plasma treatment for 5 minutes to remove the remaining organic residues and make the surface hydrophilic.

2.3. Preparation of Composite Thin Films and Single Active-layer Electrochromic Devices

20 mg of annealed MoO_3 nanoparticles were dispersed in 20 mL of DI H_2O by ultra-sonication for 4 h until a clear dispersion was obtained. As-received PEDOT: PSS dispersion was diluted to 2 mg/mL. Then 2 mg/mL of MoO_3 dispersion and 2 mg/mL of PEDOT: PSS dispersion were mixed in a volume ratio of 3:1. For comparison, composites with different ratios (1:1, 3:1, 5:1), pure MoO_3 and pure PEDOT: PSS were also prepared. The freshly mixed dispersions were dropped onto pre-cleaned ITO glasses at a heating temperature of 70 °C to obtain electrochromic films. A single active layer electrochromic device was fabricated with a sandwich configuration of ITO glass//MoO3/PEDOT: PSS//electrolyte//ITO glass. 1 M $LiClO_4$ solution was used as an electrolyte.

2.4. Characterization

The stability of the devices was examined. Fourier-transform infrared spectroscopy FTIR spectra of the MoO_3 precursor before annealing and the MoO_3 nanoparticles after annealing were recorded on a Frontier FTIR spectrometer (Perkin Elmer Frontier) in transmission mode in the range 400 to 4000 cm^{-1}. X-ray diffraction (XRD) patterns were recorded on a Bruker D8 Advance XRD. Field-emission scanning electron microscopy (FE-SEM) images of the materials were obtained on a NOVA NANOSEM 450 with secondary electron (SE) detector and low angle backscattered electron (LABE) detector. X-ray photoelectron spectroscopy (XPS) was performed using Kratos AXIS Supra. The electrochemical properties of the samples were measured in a three-electrode electrochemical cell, using the sample, Pt, and Ag as the working, counter, and reference electrodes, respectively, in 1 M $LiClO_4$ PC solution. Cyclic voltammetry (CV) was tested from -1 V to +1 V at a scan rate of 20 mV s^{-1} and electrochemical impedance spectroscopy was performed over the frequency range from 105 to 10^{-1} Hz with a signal amplitude of 5 mV using Autolab PGSTAT460 potentiostat. The in situ Spectro electrochemical properties of the samples, including UV-Vis spectra from 400 to 800 nm at different voltages and switching curves at a fixed wavelength of 600 nm, were recorded with a UV-Vis-NIR Spectrophotometer, Agilent Technologies (1AK00048809PFIZIK 2012)

3. Results and discussion

This section discussed the various experimental techniques used in this research. In terms of purpose, most of the techniques used can be divided into two main categories: techniques for characterizing the materials and techniques for testing the electrochemical properties. In the first category, the techniques used to characterize the materials include scanning electron microscopy, transition electron microscopy, X-ray diffraction, Fourier transform infrared spectroscopy. They provide the material information such as morphology, composition, crystal structure, chemical structure, particle size, zeta potential as it can be used to study the dispersion in the composite and the interfacial interactions between the two components of the composite, which are the most important factors for the performance of the composite. In the second category, to test the electrochemical performances of the composites, some electrochemical techniques are performed to study the electrochemical and electrochromic properties of the composite, such as: In situ Spectro electrochemical test, cyclic voltammetry, and electrochemical impedance spectroscopy.

3.1. Structures and Morphologies of the MoO_3/PEDOT: PSS Composites

Mo powder was dispersed in H_2O_2 to prepare the sol-gel precursor that is part of the electrochromic film fabrication process. The precursor was annealed to obtain semi-crystalline MoO_3 nanoparticles. The MoO_3 nanoparticles were then redispersed in water and mixed with PEDOT: PSS dispersion. The mixed dispersion was later used for dropping casting onto ITO glasses to make the electrochromic films and devices.

The chemical structure change of the MoO_3 precursor caused by the annealing process is confirmed by FTIR spectra. (Figure 2a) Before annealing, the FTIR spectrum shows three characteristic bands corresponding to the stretching of O=Mo at ~960 cm^{-1}, the stretching of the O-O peroxo structure at ~930 cm^{-1}, and the stretching of MoO_3 at ~560 cm^{-1} [14]. After annealing, the O-O band disappears, and a new band appears at ~876 cm^{-1} corresponding to the Mo-O-Mo stretching mode [6]. FTIR results indicate the formation of MoO3 after annealing. The band at ~1628 cm^{-1} and the broad band at 3400-3510 cm^{-1} are assigned to (H_2O) and ν(OH) respectively [7]. The presence of OH on the surface of MoO_3 nanoparticles allows them to disperse in water. The morphology of these particles at different magnification was observed by FE-SEM as shown in Figure 2c and d. Before annealing, the particles are smaller and have a broader size distribution. After annealing, MoO_3 nanoparticles are formed, which are more spherical in shape and about 10–30 nm in diameter. The crystal structure caused by the annealing process is studied by XRD. (Figure 2b) Particles originating from the precursor (before annealing) are amorphous. After annealing the precursor at 300 °C, crystallization occurs in MoO_3 (the sample is denoted MoO_3-300 °C) and the XRD pattern shows characteristic peaks of orthorhombic MoO_3 (ICDD 01-074-7912). By further increasing the annealing temperature to 500 °C, the characteristic peaks of MoO_3-500°C is at the same positions as those of MoO_3-300 °C but become sharper with a smaller full width at half maximum (FWHM), indicating higher crystallinity and larger Crystal domains indicates. However, MoO_3-500 ^{0}C cannot be redispersed in water and hence MoO_3-300 ^{o}C will be used for later studies. The semi-crystalline nature of MoO_3-300 ^{0}C is further evidenced by FE-SEM observation of the MoO_3 nanoparticles as shown in Figure 2e-f. The particle size shown in the images corresponds to the FE-SEM result and the polycrystalline structure is observed under high magnification.

The crystal lattices can be observed, and each crystal domain is about 4-10 nm in size. In summary, the prepared MoO_3 nanoparticles are highly crystalline with small particle diameters. The polycrystalline nature of the MoO_3 particles favors their electrochemical stability, while their small size facilitates their effective interactions with PEDOT: PSS.

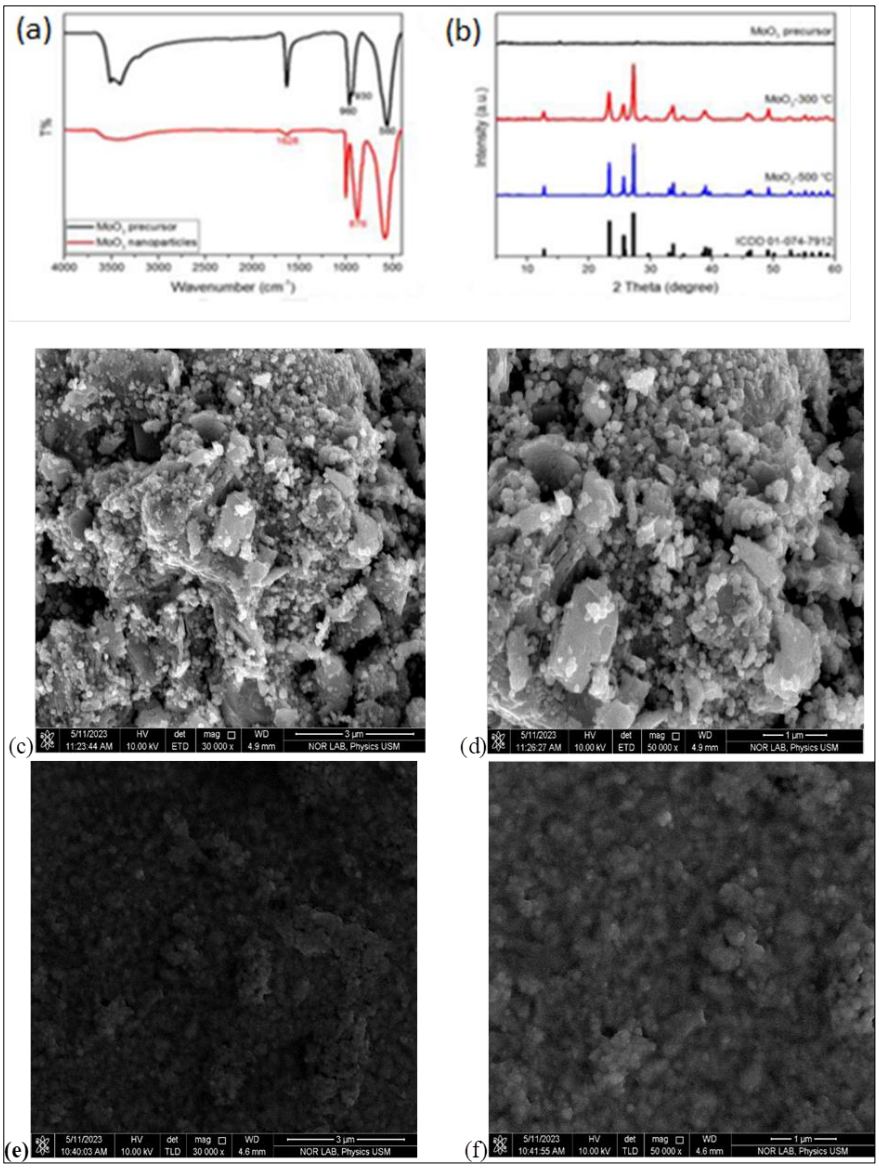

Figure 2 (a) FTIR spectra of MoO_3 precursor before annealing and MoO_3 nanoparticles after annealing. (b) XRD patterns of MoO_3 precursor, MoO_3-300 °C, MoO_3-500 °C, and reference diffraction pattern of ICDD 01-074-7912. (c) and (d) shows the Morphology of MoO_3 nanoparticles at different magnifications. (e) and (f) shows MoO_3-300 ^{0}C after annealing

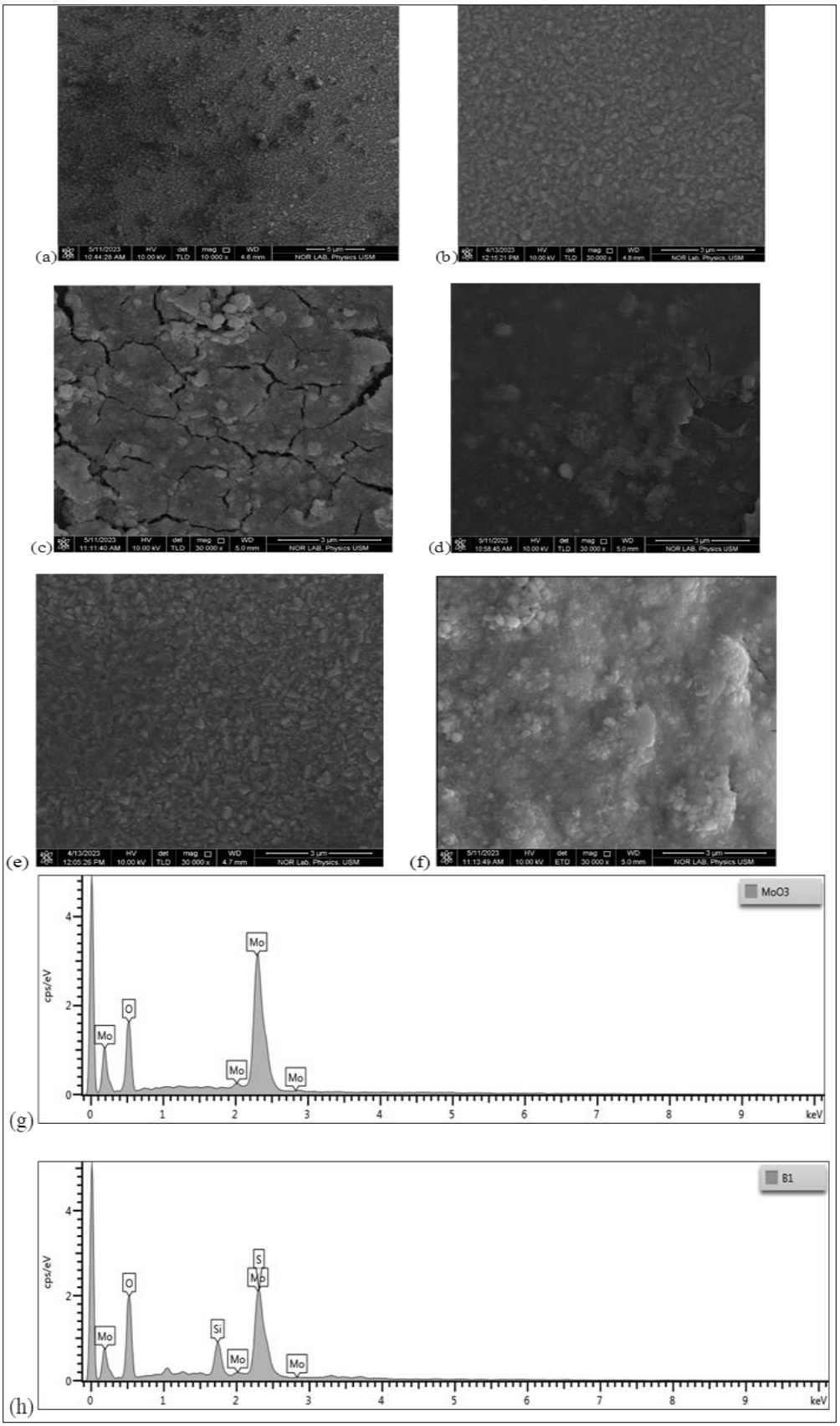

Figure 3 SEM-SEI images of (a) MoO_3, (b) PEDOT: PSS and (c) MoO_3/PEDOT: PSS; SEM-LABE images of (d) MoO_3, (e) PEDOT: PSS and (f) MoO_3/PEDOT:PSS (g) EDX of MoO3 and (h) EDX of the composite

The SEM images showing the surface morphology of MoO_3, PEDOT: PSS and MoO_3/PEDOT: PSS fabricated on ITO glasses are shown in Figure 3a-c. All three samples form smooth thin films. PEDOT: PSS and MoO_3/PEDOT: PSS films have smoother textures than MoO3 films due to the presence of a few individual isolated MoO_3 nanoparticles on top of the densely packed MoO_3 nanoparticles, which increases the roughness of the film. Apparently PEDOT: PSS can mitigate this effect due to its flexibility and conformation. In order to confirm the presence and distribution of MoO_3 nanoparticles in the composite, SEM-LABE is used to study the distribution of the MoO_3 nanoparticles in the composite, since in this case EDX is unable to detect the phase morphology (the characteristic X-ray emission of Mo (2.293 keV) has an energy very similar to that of S (2.307 keV).Under SEM-LABE, the component with the higher average atomic number appears brighter in the image. Figure 3f shows a clear composite white and black contrast, with white Areas should be MoO_3-rich Regions given pure MoO_3 and PEDOT: PSS show no contrast in their SEM-LABE images (Figure 3d-e). Figure 3f implies that MoO_3 agglomerates with an average size of about 100-200 nm in PEDOT: PSS.

3.2. Interfacial Interactions

To establish the structure-property relationship for this new composite system, the interaction between MoO_3 and PEDOT: PSS in the composite is investigated. The particle size distribution in the suspension is studied to study the interaction between MoO_3 and PEDOT: PSS particles. Under dynamic light scattering, the MoO_3 suspension has an average particle size of 165 nm and the PEDOT: PSS suspension has an average particle size of 750 nm. (Figure 4a)

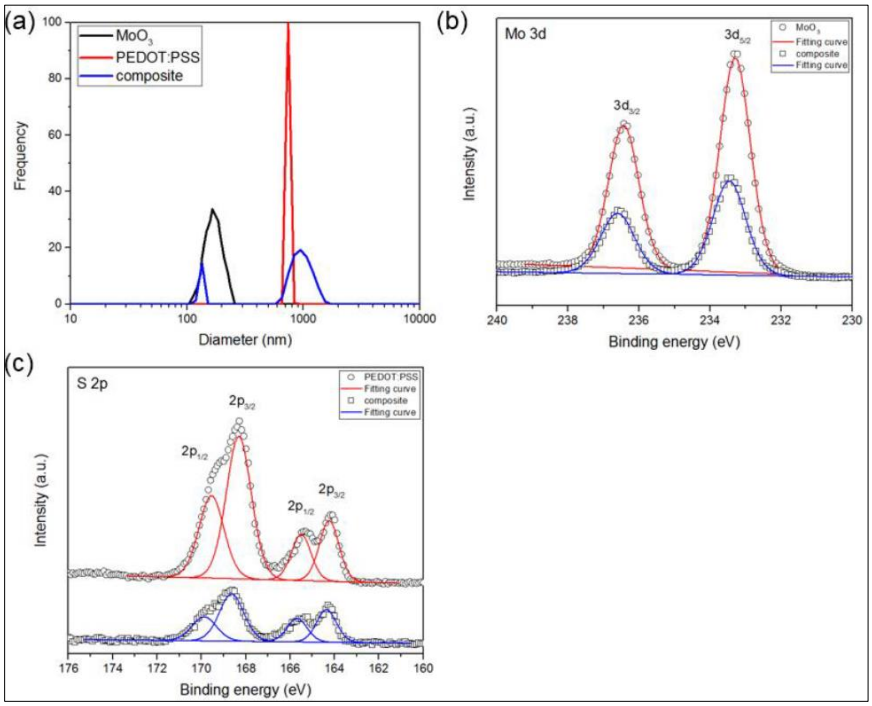

Figure 4 (a) Particle size distribution of MoO_3, PEDOT: PSS and composite tested by dynamic light scattering. XPS spectra in (b) Mo 3d region of MoO_3 and composite and (c) S 2p region of PEDOT: PSS and composite

After mixing the two suspensions by stirring, the new suspension has a bimodal size distribution with two Peaks at a particle size of 130 nm and 950 nm, respectively. The average size decrease in the first peak and the increase in the second peak indicate that some MoO_3 nanoparticles interact with PEDOT: PSS to form larger particles. The driving force of the interaction is probably electrostatic attractions [16] since MoO_3 nanoparticles are negatively charged (zeta potential: -36.3 mV) and PEDOT in PEDOT: PSS exists in the form of radical cations. To further verify the interfacial interactions, the chemical environment of Mo and S is investigated using XPS. (Figure 4b-c) For the pure MoO3, two bands at a binding energy of 236.4 eV (Mo 3d3/2) and 233.3 eV (Mo 3d5/2) correspond to the oxidation state of MO_{VI}, indicating that MO is the highest oxidation state [13]. The relatively higher binding energies than the reported values for crystalline MoO_3 can be attributed to the large amount of surface groups. The MoO_3/PEDOT: PSS composite shows two bands at 236.6 eV and 233.5 eV, which are 0.2 eV higher than pure MoO_3. In the S2p scan of PEDOT: PSS, the two bands at lower binding energy (165.5 eV, 164.2 eV) are assigned to PEDOT and the two bands at higher binding energy (169.5 eV, 168.3 eV) are assigned to PSS [11]. For the composite, the bands of PEDOT shift to positions 0.2 eV higher and the bands of PSS to positions 0.4 eV higher. This is likely due to the electrostatic attraction between negatively charged MoO_3 and positively charged S, resulting in a strong interaction between MoO_3 and PEDOT: PSS. It is more

difficult for the inner electrons to escape, which leads to a higher binding energy in the compound. It is worth noting that the shift in PSS is higher than in PEDOT, meaning more MoO_3 can interact with PSS, which is reasonable considering the core-shell structure of PEDOT: PSS.

3.3. Electrochemical Properties

The electrochemical properties of MoO_3, PEDOT: PSS and composite are further investigated by CV from -1V to +1V. (Figure 5) MoO_3 has a broad oxidation peak at -0.43 V and no obvious reduction peak in this range. PEDOT: PSS has an oxidation peak at -0.02 V and a reduction peak at -0.55 V. In the composition, the peak at -0.43 V becomes a shoulder and a new pair of redox peaks appear at -0.18 V/ -0.09 V. Based on the literature, more than a few peaks were found in the CV during the Li^+ intercalation process of MoO_3, which are attributed to the multi-step Li^+ intercalation in interlayer and intralayer spaces of MoO_3 [21]. The appearance of new peaks means that more active sites are involved in the Li^+ intercalation process, which corresponds to the larger enclosed area of the composite than that of MoO_3. Furthermore, the presence of peaks from both PEDOT: PSS and MoO_3 indicates that both components in the composite participate in the electrochemical process.

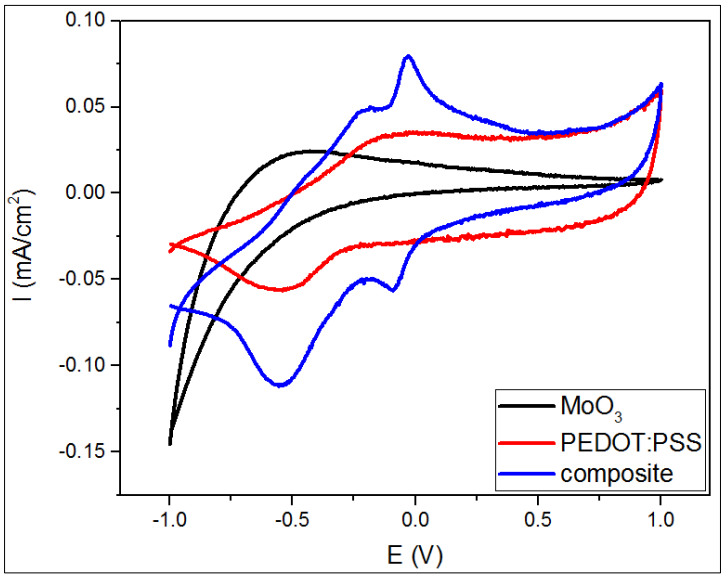

Figure 5 Cyclic voltammetry of MoO_3, PEDOT: PSS and composite from -1 V to +1 V at a scan rate of 20 mV s^{-1}

With the above analysis, the interaction between MoO_3 and PEDOT: PSS in the composite is suggested as follows. The electrostatic attraction between negatively charged surface groups of MoO_3 and positively charged S in PEDOT makes them interact with each other [16]. PEDOT: PSS has a chain structure where PEDOT is the core and PSS is the shell. Under the attraction, MoO_3 is bound to PSS due to its hydrophilicity and the structure that PEDOT is surrounded by PSS [24]. In the composite, PEDOT: PSS becomes a backbone, and MoO_3 nanoparticles are separated and attached to the backbone. Such a morphology can facilitate Li+ and electron transport in the material. Li+ and electron transport is slow in MoO_3, so only limited active sites are involved in the reaction and mainly interlayer sites are occupied. In the composite, Li+ and electron transport is faster in PEDOT: PSS. The average diffusion length to active sites in MoO_3 is reduced and replaced by the pathway in PEDOT: PSS, which has better kinetics. More active sites in MoO_3 are involved in the reaction, including both interlayer and intralayer centers.

3.4. Electrochromic Performances

The electrochromic performances of the composites and each individual component are compared in (Figure 6). Spectra of MoO_3, PEDOT: PSS, MoO_3/PEDOT: PSS at different voltages are shown in Figure 6(i-iii). The samples prepared in this way are marked with 0 V. All samples are cathodically colored materials. Their colored states are labeled -0.8V and their bleached states are labeled +0.8V. It is clearly shown that MoO_3, in contrast to PEDOT: PSS, is not able to switch back completely, although it shows a large contrast in its first staining procedure. This problem is solved when PEDOT: PSS is added, allowing MoO_3/PEDOT: PSS to fully bleach to its original state. This is attributed to the addition of PEDOT: PSS facilitates Li^+ and electron transport. The matrix formed by PEDOT: PSS provides pathways to electrons and Li^+ for inbound and outbound transport. In addition, the composite exhibits relatively constant contrast over the visible wavelength range and its maximum contrast occurs at 600 nm.

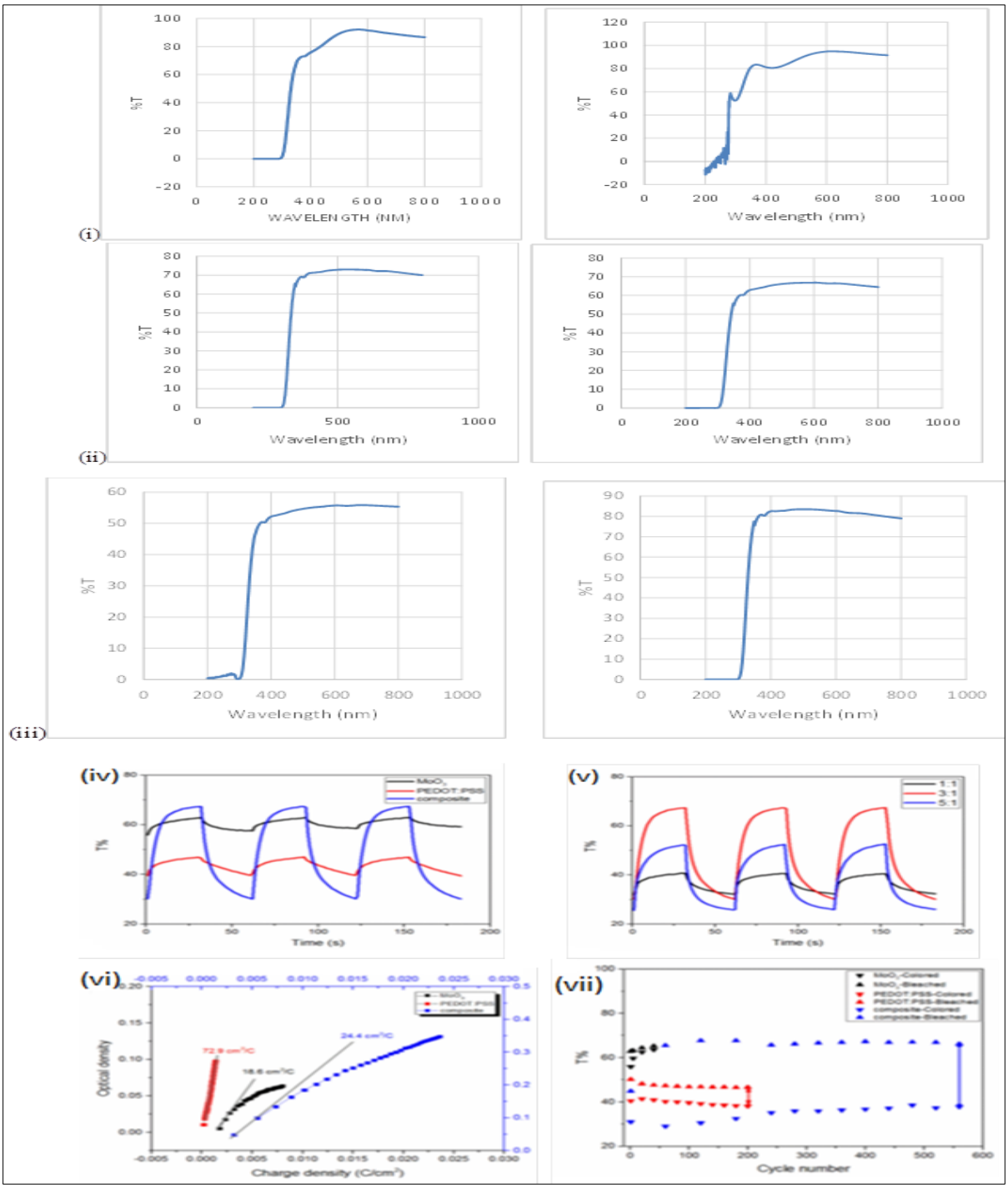

Figure 6 Electrochromic performance of MoO_3, PEDOT: PSS and composite: optical spectra of (i) MoO_3, (ii) PEDOT: PSS and (iii) composite at different potentials (-0.8 V and +0.8 V). (vi) Switching curves, (v) Switching curves of MoO_3/PEDOT: PSS composite with different component ratios of MoO_3 to PEDOT: PSS = 1:1, 3:1, and 5:1. (vi) coloration efficiencies and (vii) long-term stabilities of MoO_3, PEDOT: PSS and composite tested at 600 nm under -0.8 V, 30 s/+0.8 V, 30 s

This is closer to the wavelength (about 580 nm) most sensitive to the human eye [23] compared to the currently widely used WO_3, where the best power contrast occurs at 720 nm [36]. Therefore, it shows a clearer contrast than WO_3. Figure 6(iv) shows the switching curves of MoO_3, PEDOT: PSS, MoO_3/PEDOT: PSS at the wavelength of 600 nm after a few stabilization cycles. MoO_3/PEDOT: PSS shows the highest optical contrast of 37%, while MoO_3 and PEDOT: PSS have only 7% and 8% optical contrast, respectively. Composite samples with different ratios of MoO_3 to PEDOT: PSS (1:1, 3:1, 5:1) were tested and the sample with the 3:1 ratio has the best contrast. (Figure 6v) The bleaching/coloring time of MoO_3, PEDOT: PSS, and composite are 28 s/25 s, 21 s/26 s, and 12 s/17 s, respectively. The faster switching speed of

composites is further evidence of the improvement in the electron transport. The coloration efficiencies of MoO_3, PEDOT: PSS and composite are 18.6, 72.9 and 24.4 cm2 C^{-1}, respectively. (Figure 6vi) The long-term stabilities of all three samples are compared in Figure 6vii. MoO_3 has very poor stability and obviously breaks down after 50 cycles. MoO_3/PEDOT: PSS has a contrast of 14% in the first cycle. However, after about 60 cycles of the activation process, it gradually reaches its maximum contrast of 37%. After 240 cycles it drops to 30% and starts to stay at that number. After 550 cycles, it still retains 77% of its maximum contrast, showing better long-term stability than most of the reported MoO_3-based electrochromic materials. The good long-term stability of MoO_3/PEDOT: PSS has two reasons. One of them is PEDOT: PSS provides routes for inward and outward Li^+ transport, thus improving the problem of Li^+ trapping in MoO_3. The other is PEDOT: PSS holds the MoO_3 nanoparticles as a matrix that buffers the induced stress during the Li^+ intercalation process.

4. Conclusion

In summary, a novel MoO_3/PEDOT: PSS composite is facilely fabricated through electrostatic interactions. The small particle size of MoO_3 improves the stability of the MoO_3 nanoparticles and increases the interface significantly. The addition of PEDOT: PSS facilitates Li^+ and electron transport in and out of the MoO_3 active sites, alleviating the problem of Li^+ trapping and the resulting more active sites in MoO_3 being involved in the Li^+ intercalation process. The complementary conductivities of MoO_3 and PEDOT: PSS facilitate electron transport in both the oxidized and reduced states and are better utilized due to the extensive interfacial interactions between the two components. In addition, PEDOT: PSS acts as a polymer matrix to cushion the induced stress during cycling, benefiting long-term stability. This study addresses the critical stability issue of MoO_3 and offers MoO_3-based materials a potential for use in electrochromic applications.

Compliance with ethical standards

Disclosure of conflict of interest

No conflict of interest to be disclosed.

References

[1] Alov, N. V. (2015). XPS study of MoO3 and WO3 oxide surface modificatin by low-energy Ar ion bombardment. Physics Status Solide, 4, 1–4. https://doi.org/10.1002/pssc.201400108

[2] Anna, M. O., Shen, D. E., Kerszulis, J. A., Bulloch, R. H., Kuepfert, M., Dyer, A. L., & Reynolds, J. R. (2015). Four Shades of Brown: Tuning of Electrochromic Polymer Blends Toward High-Contrast Eyewear. ACS Applied Materials and Interfaces. https://doi.org/10.1021/am507063d

[3] Atak, G., & Duyar Coskun, O. (2017). Annealing effects of NiO films for all-solid-state electrochromic devices. Solid State Ionics, 305(May), 43–51. https://doi.org/10.1016/j.ssi.2017.05.002

[4] Au, B. W., & Chan, K. (2019). Effect of precursor solution stirring time on the electrochromic performance of tungsten oxide films. Surface Engineering, 0(0), 1–6. https://doi.org/10.1080/02670844.2019.1622264

[5] Bae, J., Koo, B., & Ahn, H. (2018). Fe doping effect of vanadium oxide films for enhanced switching electrochromic performances. Ceramics International. https://doi.org/10.1016/j.ceramint.2018.12.219

[6] Bhatia, S., Khanna, A., & Jain, R. K. (2019). Structure-property correlations in molybdenum trioxide thin films and nanoparticles Structure-property correlations in molybdenum trioxide thin fi lms and nanoparticles. Materials Research Express, 6, 0–17. https://doi.org/https://doi.org/10.1088/2053-1591/ab1855

[7] Castables, N. R., & Madej, D. (2020). In Situ Spinel Formation in a Smart Nano -Structured Matrix for No-cement refractory castables. Materials, 13(1403). https://doi.org/10.3390/ma13061403

[8] Chang-jian, C., Cho, E., Yen, S., Ho, B., & Lee, K. (2018). Dyes and Pigments Facile preparation of WO 3 / PEDOT : PSS composite for inkjet printed electrochromic window and its performance for heat shielding. Dyes and Pigments, 148, 465–473. https://doi.org/10.1016/j.dyepig.2017.09.026

[9] Guofa, C., Peter, D., Mengqi, C., Jiangwei, C., Shlomo, M., & See Pooi, L. (2016). Highly Stable Transparent Conductive Silver Grid / PEDOT : PSS Electrodes for Integrated Bifunctional Flexible Electrochromic Supercapacitors. Advance Energy Materials. https://doi.org/https://doi.org/10.1002/aenm.201501882

[10] Hernández-labrado, G. R., Contreras-donayre, R. E., Collazos-castro, J. E., & Polo, J. L. (2011). Subdiffusion behavior in poly (3 , 4-ethylenedioxythiophene): Polystyrene sulfonate (PEDOT : PSS) evidenced by electrochemical impedance spectroscopy. Journal of Electroanalytical Chemistry, 659, 201–204. https://doi.org/10.1016/j.jelechem.2011.05.008

[11] Jenkins, M. J., Carter, J. L., Kelly, C. A., Marshall, J. E., Hammond, V., Goodship, V., … Goodship, V. (2022). PEDOT : PSS Conductivity Enhancement Through Addition of the Surfactant Tween 80 Enhancement through Addition of the Surfactant. Polymers, 14, 5072. https://doi.org/https://doi.org/10.3390/polym14235072

[12] Jeong, K. R., Lee, I., Park, J. Y., Choi, C. S., Cho, S., & Lee, J. (2017). Enhanced black state induced by spatial silver nanoparticles in an electrochromic device. NPG Asia Materials, 9(3), e362-8. https://doi.org/10.1038/am.2017.25

[13] Lee, K., Sun, S., Ko, H., Beom, S., Lee, G., Lee, D., … Paik, U. (2023). Modulation of Molybdenum oxidation state via Catalytic-oxidation. Applied Surface Science, 615(January), 156330. https://doi.org/10.1016/j.apsusc.2023.156330

[14] Liao, X., Jeong, A. R., Wilks, R. G., Wiesner, S., Rusu, M., Felix, R., … Bar, M. (2019). Tunability of MoO 3 Thin-Film Properties Due to Annealing in Situ Monitored by Hard X - ray Photoemission. ACS Omega, 4, 10985–10990. https://doi.org/10.1021/acsomega.9b01027

[15] Liu, Y., Lv, Y., Tang, Z., He, L., & Liu, X. (2016). Highly stable and fl exible ITO-free electrochromic fi lms with bi-functional stacked MoO 3 / Ag / MoO 3 structures. Electrochimica Acta, 189, 184–189. https://doi.org/10.1016/j.electacta.2015.12.115

[16] Maniruzzaman, M., Abdur, R., sheikh Kuddus, M. A., Singh, S., & Lee, J. (2023). Conductive MoO 3 –PEDOT:PSS Composite Layer in MoO 3 /Au/MoO 3 –PEDOT:PSS Multilayer Electrode in ITO-Free Organic Solar Cells. Processes, 11(594). https://doi.org/https://doi.org/10.3390/pr11020594

[17] Mei, B., Munteshari, O., Lau, J., Dunn, B., & Pilon, L. (2018). Physical Interpretations of Nyquist Plots for EDLC Electrodes and Devices. PHYSICAL CHEMISTRY C, 122, 194–206. https://doi.org/10.1021/acs.jpcc.7b10582

[18] Meng, Q., Jiang, Q., Cai, K., & Chen, L. (2019). Preparation and thermoelectric properties of PEDOT : PSS coated Te nanorod / PEDOT : PSS composite films. Organic Electronics, 64(October 2018), 79–85. https://doi.org/10.1016/j.orgel.2018.10.010

[19] Moghazy, M. A. (2023). Leidenfrost green synthesis method for - MoO 3 and - WO 3 nanorods preparation : characterization and methylene blue adsorption ability. BMC Chemistry, 1–11. https://doi.org/10.1186/s13065-023-00916-3

[20] Monk, P. M. S., Mortimer, R. J., & Rosseinsky, D. R. (2007). No Title. Retrieved from www.cambridge.org/9780521822695

[21] Ng, D. H. L., Li, S., Li, J., Huang, J., Cui, Y., Lian, J., & Wang, C. (2022). Storage of Lithium-Ion by Phase Engineered MoO 3 Homojunctions. Nanomaterials, 12(3762), 1–9. https://doi.org/https://doi.org/10.3390/nano12213762

[22] Pan, M., Ke, Y., Ma, L., Zhao, S., Wu, N., & Xiao, D. (2018). Single-layer electrochromic device based on hydroxyalkyl viologens with large contrast and high coloration efficiency. Electrochimica Acta. https://doi.org/10.1016/j.electacta.2018.01.206

[23] Roman, A. J., Powers, C. A., Semenov, E. P., Sheplock, R., Aksianiuk, V., Russell, R. C., … Jacobson, S. G. (2019). Short-Wavelength Sensitive Cone (S-cone) Testing as an Outcome Measure for NR2E3 Clinical Treatment Trials. International Journal of Molecular Sciences, 20(2497). https://doi.org/10.3390/ijms20102497

[24] Sanchez-Vergara, M., Hamui, L., Gonz, D., & Cosme, I. (2021). Efficient Film Fabrication and Characterization of Poly(3,4-ethylenedioxythiophene):Poly(styrenesulfonate) (PEDOT:PSS)-Metalloporphine Nanocomposite and its Application as Semiconductor Material. Polymers, 13(4008). https://doi.org/https://doi.org/10.3390/polym13224008

[25] Shankar, S., Lahav, M., & Boom, M. E. Van Der. (2015). Coordination-Based Molecular Assemblies as Electrochromic Materials: Ultra-High Switching Stability and Coloration Efficiencies. AMERICAN CHEMICAL SOCIETY, 2–5. https://doi.org/10.1021/jacs.5b00429

[26] Thakur, V. K., Ding, G., Ma, J., Lee, P. S., & Lu, X. (2012). Hybrid Materials and Polymer Electrolytes for Electrochromic Device Applications. ADVANCE MATERIALS, 1–26. https://doi.org/10.1002/adma.201200213

[27] Wang, D., Wei, L., Shi, P., Chen, Y., Yan, S., Tian, Y., & Jiao, J. (2018). Electrochromic behavior of fluorine-doped tin oxide film via guided motion of Li ions. Journal of Alloys and Compounds. https://doi.org/10.1016/j.jallcom.2018.08.268

[28] Wang, Q., Zhou, H., Wang, S., & Hu, C. (2016). Structure, stability and electrochromic properties of polyaniline film covalently bonded to indium tin oxide substrate. Applied Surface Science. https://doi.org/10.1016/j.apsusc.2016.01.041

[29] Wang, Y., Zheng, R., Luo, J., Malik, H. A., Wan, Z., Jia, C., … Yao, X. (2019). Self-healing dynamically cross linked versatile polymer electrolyte: A novel approach towards high performance, flexible electrochromic devices. Electrochimica Acta. https://doi.org/10.1016/j.electacta.2019.06.182

[30] Welsh, B. D. M., Kumar, A., Meijer, E. W., & Reynolds, J. R. (1999). Enhanced Contrast Ratios and Rapid Switching in Electrochromics Based on Poly (3 , 4-propylenedioxythiophene) Derivatives **. 1379–1382.

[31] Wu, W., Wang, M., Ma, J., Cao, Y., & Deng, Y. (2018). Electrochromic Metal Oxides : Recent Progress and Prospect. ADVANCE ELECTRONIC MATERIALS, 1800185, 1–19. https://doi.org/10.1002/aelm.201800185

[32] Xia, X., Chao, D., Qi, X., Xiong, Q., Zhang, Y., Tu, J., … Fan, H. J. (2013). Controllable Growth of Conducting Polymers Shell for Constructing High-Quality Organic/Inorganic Core/Shell Nanostructures and Their Optical-Electrochemical Properties. NANO LETTERS. https://doi.org/dx.doi.org/10.1021/nl402741j

[33] Yan, C., Kang, W., Wang, J., Cui, M., Wang, X., Foo, C. Y., … Lee, P. S. (2013). Stretchable and Wearable Electrochromic Devices. ACS NANO, (Xx).

[34] Zhang, S., Chen, S., Yang, F., Hu, F., Yan, B., Gu, Y., … Xiang, M. (2018). High-performance electrochromic device based on novel polyaniline nanofibers wrapped antimony-doped tin oxide/TiO2 nanorods. Organic Electronics. https://doi.org/10.1016/j.orgel.2018.11.036

[35] Zhang, X., Yang, W., Zhang, H., Xie, M., & Duan, X. (2022). PEDOT : PSS : From conductive polymers to sensors. Nanotechnology and Precision Engineering, 4(045004). https://doi.org/10.1063/10.0006866

[36] Zhao, Y., Zhang, X., Li, W., Li, Z., Zhang, H., Chen, M., … Li, Y. (2022). High-performance electrochromic WO 3 film driven by controllable crystalline structure and its all-solid-state device. Solar Energy Materials and Solar Cells, 237(November 2021), 111564. https://doi.org/10.1016/j.solmat.2021.111564